Cavendish–HEP–97/04
June 1997
Revised November 1997

Single-top production at future ep colliders

Stefano Moretti[1] and Kosuke Odagiri[1]

Cavendish Laboratory, University of Cambridge,
Madingley Road, Cambridge, CB3 0HE, United Kingdom.

Abstract

The production of top quarks in single mode at future ep colliders is studied, the attention being mainly focused to the case of the proposed LEP$\oplus$LHC collider. We are motivated to reanalyse such a process following the discovery of the top quark at Fermilab. Thanks to the measurement of its mass one is now able to establish more accurately the relevance of single top production for itself and for many other processes to which it may act as a background. In addition, the recent improvement of our knowledge of the quark and gluon dynamics inside the proton now allows one to pin down the dependence of single top production on the partonic structure functions. Both the leptonic and hadronic decay channels of the top quark are studied and compared to the yield of the corresponding irreducible background in presence of b-tagging.

[1]E-mail: moretti, odagiri@hep.phy.cam.ac.uk

1. Introduction

Now that the Fermilab experiments have clearly assessed the existence of the heaviest quark of the Standard Model (SM) [1] and given a rather accurate measurement of its mass [2], many of the theoretical calculations carried out in the previous years need to be updated to the current value of this fundamental parameter. In this paper, we turn our attention to the case of top production in single mode at future electron(positron)-proton colliders. As a further motivation for our revision we put forward the fact that a huge amount of data improving our knowledge of the parton distribution functions (PDFs) has been produced in the years following the early studies of top phenomenology at *ep* machines (see, e.g., Ref. [3]), along with more detailed treatments of the dynamics of heavy quarks inside the proton. Therefore, the error associated with the partonic behaviour in the initial state should be at present significantly smaller than in the past. Finally, the reduction of the theoretical uncertainty in single top production also implies that other effects, such as those due to the irreducible backgrounds, need now to be incorporated in more detailed phenomenological analyses. We calculate these effects here for the first time, in both the hadronic and leptonic top decay channels.

In order to illustrate the particular relevance of single top processes in electron(positron)-proton scatterings we remind the readers of the motivations for higher energy *ep* experiments.

Firstly, such colliders will be an obvious and unrivaled testing ground for QCD at very low Bjorken x [4], in exploring the structures of both the proton and the photon [5] at the TeV scale, taking over the presently running HERA machine [6]. In connection with this point, we will show that the single top quark process discussed here can be useful in understanding the phenomenology of the PDF of the bottom quark.

Secondly, and particularly in the case of the proposed LEP$\oplus$LHC collider [3], they will be able to search for the Higgs boson ϕ of the Standard Model [7] (or the lightest neutral Higgs boson of the Minimal Supersymmetric Standard Model, MSSM) in the intermediate mass range 90 GeV $\lesssim M_\phi \lesssim$ 130 GeV [8, 9], in the case it may not be accessible at the LHC nor the existing colliders (see Ref. [10] for discussions on this point). As was discussed in [7], the jet background due to the top quark will be large if only a single b-tagging is implemented in identifying the Higgs boson decay in the most favoured channel $ep \to \nu_e W^+W^-X \to \nu_e \phi X \to \nu_e b\bar{b}X$ [7].

Thirdly, the rôle of an *ep* machine will be complementary to those of e^+e^- (i.e., NLC) and *pp* (i.e., LHC) colliders in the search for New Physics such as leptoquarks, excited leptons, low mass sleptons, doubly charged Higgs bosons, and new vector bosons (see [4] and the references therein). Many of these processes have neutral current-type interactions of the form $eq \to eq$, and so the single top quark process, when the top quark decays leptonically to a bottom quark, a positron and an electron neutrino, is a potentially dangerous background which should be included in experimental simulations. As for the possibility of exotic top quark decays, the study of the Supersymmetric two-body decay modes is a straightforward extension of this project [11] and will be carried out elsewhere [12].

Although the physics potential of a higher energy *ep* machine is suppressed compared to a *pp* one by the reduced centre-of-mass (CM) energy and luminosity, we stress its allure in the suppression of the initial state QCD noise, which allows for a cleaner environment to study the physics of the TeV scale, possibly before an NLC will be in operation [13]. We also mention that the physics of ep colliders, in conjunction with the possibility of their running in the γp mode [14], has been recently under renewed and active discussion [15].

The production of top quarks at future ep colliders [3] has been studied in the context of top quark searches at LEP1⊕LHC [4], during the 1990 Aachen Workshop. A detailed study was presented in the corresponding Proceedings [16]. There, the two following channels were investigated [17]:

$$\text{CC:} \qquad W^{\pm} + g \to tb, \tag{1}$$

$$\text{NC:} \qquad \gamma, Z + g \to t\bar{t}, \tag{2}$$

via charged (CC) and neutral current (NC) scatterings of an off-shell gauge boson against a gluon, the former being produced via bremsstrahlung off the incoming electron(positron) and the latter being extracted from the proton. In general, the CC channel dominates over the NC one, due to the larger phase space available. For $m_t = 175$ GeV [2], the suppression is more than one order of magnitude at the TeV scale [16]. (Indeed, this is the reason why we will concentrate on $W^{\pm}g$ fusion only.) In Ref. [16], also a detailed signal-to-background analysis was carried out, in both the (semi)leptonic and hadronic top decay channels.

The Feynman diagrams describing reaction (1) induced, e.g., by positron beams, can be found in Figure 1a, where the top is considered on-shell. As the bottom mass is small compared to m_t, the dominant contribution to the total cross section comes from diagram 1 of Figure 1a, when the final $\bar{b}$ quark is collinear with the incoming gluon. The collinear divergences are however regulated by the finite value of the bottom mass and manifest themselves by means of contributions of the form $L = \alpha_s(\mu^2)\log(\mu^2/m_b^2)$, with $\mu^2 \sim \hat{s}$, being $\hat{s}$ the CM energy at the 'partonic' level e^+b and α_s the strong coupling constant.

Such logarithms are rather large, thus terms of the form $\alpha_s^n(\mu^2)\log^n(\mu^2/m_b^2)/n!$ have to be resummed to all orders in perturbation theory [18] in order to compute the cross section reliably. This can be done by introducing a b parton distribution, $f_b(x,\mu^2)$, in terms of the Dokshitzer-Gribov-Lipatov-Altarelli-Parisi (DGLAP) splitting function

$$P_{bg}(z) = \frac{1}{2}[z^2 + (1 - z^2)] \tag{3}$$

of a gluon into $b\bar{b}$ pairs (z being the fractional energy carried away by the (anti)quark). In fact, bottoms are not valence quarks, rather they materialise once the energy scale μ of the evolution reaches their production 'threshold' at a given value $\mu_b \sim m_b$. The function $P_{bg}(z)$ is indeed the 'coefficient function' of the logarithmically enhanced term. The b structure function then evolves with μ according to the DGLAP equations, from an initial condition of the sort, e.g., $f_b(x,\mu^2) = 0$ if $\mu^2 \leq \mu_b^2$.

It follows then that single top production and decay via process (1) can be conveniently studied by computing the transition amplitude squared for the reaction (e.g., assuming incoming positron beams)

$$e^+b \to \bar{\nu}_e t \to \bar{\nu}_e bW^+ \to \bar{\nu}_e bf\bar{f}', \tag{4}$$

where f represents a lepton/neutrino or a u, d, s and c quark (produced in the top decay), appropriately convoluted with a b distribution function evaluated at the adopted scale μ^2. We exploit here this approach.

In our opinion, such a procedure (in which the parton is b) is more appropriate than the one exploited in Ref. [16] (in which the parton is g), especially at high energies. In fact, we have explicitly verified that for the values of $\sqrt{s_{ep}}$ considered here the dominant contribution to process (1) comes from configurations in which the $\bar{b}$ is collinear with the incoming gluon. Since it is exactly such emission that is summed to all orders in perturbation theory in leading and next-to-leading logarithmic accuracy inside the b structure function when $\alpha_s(\mu^2)\log(\mu^2/m_b^2) \sim \mathcal{O}(1)$ (and this is clearly the case in our context, e.g., when $\mu^2 = \hat{s} \gtrsim m_t^2$), our approach will give a more accurate answer. However, for comparison, we will also show in the present paper several rates as produced by the process induced by $g \to b\bar{b}$ splitting[2].

In this paper we study the single top quark production via e^+b fusion at various energies, together with all tree-level irreducible background processes as shown in Figures 1b, 1c and 1d. Figure 1b corresponds to the case of the leptonic decays of the $W^\pm$ boson in the signal process,

$$e^+b \to \bar{\nu}_e b \ell^+ \nu_\ell, \tag{5}$$

where $\ell = e, \mu, \tau$, whereas Figure 1c refers to hadronic decays of the $W^\pm$ boson,

$$e^+b \to \bar{\nu}_e b \ell^+ jj', \tag{6}$$

where jj' represents a pair of light quark jets $u\bar{d}$ or $c\bar{s}$. To these must be added the case of the gluon mediated background of Figure 1d,

$$e^+b \to \bar{\nu}_e b \ell^+ jj', \tag{7}$$

where jj' again represents a pair of light quark jets [3].

In addition to these three, if charge measurements of the bottom quarks prove impractical or impossible, we will have background from processes of the forms:

$$e^+\bar{b} \to \bar{\nu}_e \bar{b} \ell^+ \nu_\ell, \tag{8}$$
$$e^+\bar{b} \to \bar{\nu}_e \bar{b} \ell^+ jj'. \tag{9}$$

A single b-tagging capability is assumed throughout, all results being linearly proportional to its efficiency. The case $\ell = \tau$ assumes that jets coming from the tau and

[2]Note that the complete next-to-leading (NLO) corrections to $W^\pm g/b$ fusion involving the collinear logarithms as well as the large angle emission and the loop diagrams have been recently presented in the $\overline{\mathrm{MS}}$ renormalisation scheme [19]. Such results contradict earlier ones based on the DIS factorisation scheme [20]. For the case of ep collisions at HERA they amount to approximately 2% of the result obtained by means of the b structure function approach, and they are rather insensitive to collider energies in the TeV range. Therefore we expect them to be well under control also at the proposed LEP$\oplus$LHC, so for the time being we do not include them in our calculation. Another reason for doing so is that we will also be concerned with the interplay between the single top signal and the non-resonant irreducible background, which is here computed at lowest order.

[3]The interference between the two processes (6)–(7) vanishes identically because of colour conservation.

the quarks will easily be distinguishable. We perform all calculations for the case of e^+p colliders, although the e^-p case is precisely identical since the calculations involve no valence quarks and are therefore invariant under the exchange $e^+ \leftrightarrow e^-$.

The plan of this paper is as follows. In Section 2, we describe the methods we adopted in the calculations of the signal and background processes. In Section 3, we present and discuss our results. Section 4 is a brief summary.

2. Calculation

The tree-level Feynman diagrams that one needs in order to compute processes (5), (6) and (7) are given in Figures 1b, c and d, respectively. For reaction (5) we show the diagrams for the case $\ell = e$, which is the most complicated. When $\ell = \mu$ or τ only ten out of the twenty-one diagrams in Figure 1b contribute. For processes (6)–(7) the number of diagrams is independent of the flavour j[4].

The single top quark signals (4) are produced by diagrams 11 in Figure 1b and 4 in Figure 1c, for leptonic and hadronic $W^\pm$ decays, respectively. The remaining diagrams in Figures 1b and 1c represent the 'irreducible' background to single-top production and decay. Reaction (7) does not contribute to the signal at all, but only to the background.

Graphs in Figures 1b, c and d refer to the case of e^+b fusion, i.e., to the scattering of a positron and a bottom quark, the latter being extracted from the incoming proton beam. As mentioned earlier on, we have treated the bottom quark as a constituent of the proton with the appropriate momentum fraction distribution $f_b(x,\mu^2)$, as given by our partonic structure functions. It can be noted that the bottom antiquark is also present inside the proton with an equal probability. When calculating rates for single-top production at e^+p colliders, diagrams initiated by bottom antiquarks must also be considered. However, as long as the deep inelastic scattering of the proton takes place against a positron, such graphs do not produce a resonant top quark. The topologies of these bottom antiquark initiated graphs are easily deducible from those in Figures 1b and c. From the point of view of top quark studies, these act as additional backgrounds. Their production rates will be different from the case of e^+b fusion if the CM energy at partonic level (i.e., $\sqrt{\hat{s}}$) spans the top quark production threshold. In contrast, the cross sections due to $e^+\bar{b}$ initiated diagrams and proceeding via QCD interactions are identical to the yields of reaction (7) and the actual graphs are the same as those in Figure 1d, apart from the trivial operation of reversing the bottom quark line[5].

The possibility of the '$2b$' charged current processes $e^+q \to \bar{\nu}_e b\bar{b}q$ (where q is d, $\bar{u}$, s or $\bar{c}$) being mistagged as a single b event and acting as background to the hadronic channel can not be neglected, even when the b-tagging efficiency is high. If the latter is denoted by ϵ_b, then the probability of misidentification is given by $2\epsilon_b(1-\epsilon_b)$, assuming

[4]We will refer to process (5) as the 'leptonic' channel, and to processes (6) and (7) as the 'hadronic' channels. For the latter cases, we will further distinguish between 'electroweak' (EW) and 'strong' (QCD) production, respectively.

[5]Note that for the case of e^-p scattering things work in a complementary way, the resonant top antiquarks being produced by incoming $\bar{b}$ partons. Indeed, as bottom (anti)quarks are produced inside the nucleon via a $g \to b\bar{b}$ splitting (that is, they are sea partons), no differences occur in the deep-inelastic dynamics of the above processes if antiproton beams are considered. Although we study positron-proton colliders here, our discussions are transposable to all the other cases.

no correlations between the two b-taggings. Thus the suppression of the $2b$ background with respect to the single b events is $2(1-\epsilon_b)$. As our investigations concern mainly the top quark signal process (4), the complete analysis of single bottom quark processes being outside the scope of our present study, we content ourselves with an estimate of the degree to which this additional 'irreducible' background could affect the top quark and $W^\pm$ boson mass reconstruction (the $2b$ background does not contribute to the leptonic case). Our explicit calculation, using the methods explained below, shows that after cuts in the reconstructed top quark and $W^\pm$ boson masses are introduced, the cross section of the $2b$ process is of the same order as that of reaction (7) (differing only by 10% at the LEP$\oplus$LHC energies), thus being quite small in the end (see Section 3.).

To calculate the squared amplitudes for processes (5)–(7) we have used the `FORTRAN` packages MadGraph [21] and HELAS [22]. The codes produced have been carefully checked for gauge and BRS [23] invariance at the amplitude squared level. The multi-dimensional integrations over the phase spaces have been performed numerically using the Monte Carlo routine VEGAS [24], after folding the partonic differential cross sections with the appropriate quark densities. The programs that we have produced have been run on a DEC 3000 Model 300 alpha-station, on which the evaluation of, e.g., 10^6 events took some 14 minutes of charged CPU time to produce a cross section at the level of percent accuracy in the case of process (5) for the sum of the two contributions $\ell = e$ and μ (the latter being equivalent to the case $\ell = \tau$): that is, for the channel involving the largest number of diagrams and the most complicated resonance structure.

All the codes implemented are available from the authors upon request. To allow for a prompt evaluation of single-top rates at any energy and for any choice of selection cuts, we have also calculated the amplitude squared of process (4) analytically, including top width effects. In the leptonic case, and assuming all lepton and neutrino masses to be zero, it reads as follows[6]:

$$\overline{|M_{e^+b\to\bar{\nu}_e b'\ell^+\nu_\ell}|}^2 = 2(4\pi\alpha_{em}/\sin^2\theta_W)^4|P_{W^*}|^2|P_W|^2|P_t|^2 p_b\cdot p_{\bar{\nu}_e}(-p_e\cdot p_\ell p_t^2 + 2p_e\cdot p_t p_\ell\cdot p_t)$$

with

$$P_{W^*} = 1/(p_{W^*}^2 - M_{W^\pm}^2), P_W = 1/(p_W^2 - M_{W^\pm}^2 + iM_{W^\pm}\Gamma_{W^\pm}), P_t = 1/(p_t^2 - m_t^2 + im_t\Gamma_t)$$

$$p_{W^*} = p_e - p_{\bar{\nu}_e}, \qquad p_W = p_\ell + p_{\nu_\ell}, \qquad p_t = p_b + p_{W^*}.$$

In the hadronic case, again assuming zero light quark masses, the above formula needs to be multiplied by the colour factor 3, and ℓ^+ and ν_ℓ replaced by $\bar{d}(\bar{s})$ and $u(c)$ respectively.

The bottom quark sea distributions are not measured by experiment, but are obtained from the gluon distributions splitting into $b\bar{b}$ pairs by using the DGLAP evolution

[6]The analytic expression for process (1), also involving the decay currents, can be found in Ref. [25]. We have checked our ME for the gluon induced process against that given in Ref. [25] in the appropriate configuration (i.e., for $p\bar{p}$ collisions) and found perfect agreement.

equations [26]. Therefore, the b structure functions are different from the light quark distributions, which do need to be measured as they involve non-perturbative QCD, for which a consistent theoretical framework does not exist. In contrast, the PDFs of b quarks evolve at energies of the order of the fermion mass m_b or larger, so that their dynamics can be calculated by using the well assessed instruments of perturbative QCD. That is, given the PDFs of the gluon and of the light quarks, those of the b are precisely determined, as they do not contain any free parameters (apart from m_b, of course).

We think that by the time that ep colliders at the TeV scale will begin to be operative, the uncertainty on the gluon distributions at medium and small x may be expected to be significantly smaller than at present, principally due to forthcoming improved measurements of the small x deep inelastic structure functions at HERA, and of large p_T jet and prompt photon production at the $p\bar{p}$ (Di-)Tevatron at Fermilab and the pp LHC at CERN (the latter being scheduled to start running around 2005)[7]. Therefore, detailed studies of single top events produced in electron-proton collisions will allow one to constrain the error related to the dynamics of the $g \to b\bar{b}$ splitting in the DGLAP evolution. In fact, we expect the experimental information on b structure functions as collected at the end of the HERA, Fermilab and LHC epoch to be rather poor, if not inexistent. On the one hand, at the CM energy typical of the ep accelerator now running at DESY ($\sqrt{s}_{ep} = 314$ GeV) the content of b quark inside the scattered hadron is very much suppressed per se. On the other hand, at both the Tevatron ($\sqrt{s}_{p\bar{p}} = 1.8 - 2$ TeV) and LHC ($\sqrt{s}_{pp} = 10 - 14$ TeV) the study of b induced processes inevitably proceeds through either the production of top quarks in single mode [27], whose signatures suffer from a huge background due to $t\bar{t}$ production via $q\bar{q}$ and gg fusion, or via pure QCD interactions, biased by a large amount of light quark and gluon jet noise. These two problems can in principle be solved by future ep colliders. Firstly, they will be operating at the TeV scale thus allowing for a very much enhanced content of initial b quarks, which can be probed in the 'kinematically' more defined context of a DIS process of an electron(positron) against a proton. Secondly, as discussed previously, the single top mode via $e^{\pm}p$ collisions has a much larger cross section than top-antitop production induced by γg and/or Zg fusion [16].

As default set of PDFs in most of the results presented in this analysis we have used the LO set CTEQ(4L), together with the one-loop expression for α_s. We have done so for reasons of consistency, as the hard scattering processes have been computed here at lowest order. However, as one of the motivations of this study is to investigate the dependence of process (4) on the evolution of the structure functions of bottom quarks inside the proton, we have produced our results for other 25 recent NLO PDFs which give excellent fits to a wide range of deep inelastic scattering data and to others from different hard scattering processes (see the original references for details). These are the packages MRS(A, A', G, J, J', R1, R2, R3, R4), MRS(105, 110, 115, 120, 125, 130), MRRS(1,2,3) and CTEQ(2M, 2MS, 2MF, 2ML, 3M, 4M, 4HQ) [28]–[37]. Note that in each case the appropriate value of $\Lambda_{\mathrm{QCD}} \equiv \Lambda^{(n_f)}_{\overline{\mathrm{MS}}}$ was used. For these NLO sets, the QCD strong coupling constant α_s was in general evaluated at two-loop order at the

[7]In fact, the typical x values probed via process (4), e.g., at the LEP$\oplus$LHC, are of the order $m_t^2/\hat{s}$ or more, that is above 10^{-2}, where the gluon density is already well known at present.

scale $\mu = \sqrt{\hat{s}}$. The same choice has been made for the scale of all the mentioned LO and NLO structure functions.

In order to estimate the theoretical uncertainty related to the b quark distribution inside the proton, we will make use of the NLO sets. The spread of the corresponding results as obtained from the different packages (rather than the errors of the numerical integrations associated to the CTEQ(4L) set) can be taken as a possible estimate of the uncertainty of our predictions throughout the all paper[8]. The choice of using NLO sets in the estimation of the theoretical uncertainty is guided, on the one hand, by the fact that we will only be interested in relative differences between the various predictions (so that any bias due to the use of LO MEs vs. NLO PDFs should be expected to be quantitatively similar for all sets), and, on the other hand, by the following considerations.

Historically, there were two theoretically consistent methods of introducing bottom quarks in scattering processes: namely, as a massless (1.) or as a massive (2.) quark.

1. In this case, on the same footing as the u, d, s and c flavours, a PDF is assigned to the b quark. At NLO in α_s, one has to consider the case $g \to b\bar{b}$, whose collinear singularity (see Section 1.) is customarily factorised into the bare bottom PDF, after appropriate renormalisation of the (linear) pole. The residual (finite) contribution is a part of the NLO corrections to the partonic cross section. This way, heavy quarks in the final state can (also) be obtained by exciting the corresponding flavour inside the proton (i.e., 'flavour excitation'), as is the case here. In this treatment, the only dependence on m_b enters in defining the threshold at some point $\mu_b \sim m_b$.

2. In this scenario, the b (and c as well) quark has no PDF: only the 'light' flavours u, d and s participate in the parton dynamics inside the proton and heavy flavours can only be created in scattering processes (i.e., 'flavour creation'). At high energies, this treatment introduces in case of $g \to b\bar{b}$ splittings the large logarithms mentioned in the previous Section.

The latter is often referred to as the TFN-scheme, where TFN stands for *Three-Flavour-Number* (such as in the GRV [38, 39] sets) whereas the former is the so-called FFN-scheme, where FFN stands for *Four(and Five)-Flavour-Number* (such as in the MRS and CTEQ sets). These two treatments are somewhat 'complementary', as it turns out that (see, e.g., Ref. [40]) the TFN-scheme is the most suitable for the heavy quark component of the PDFs near threshold whereas well above this regime (where the finite value of m_q, with $q = c, b$, has small numerical impact) is the FFN-scheme that should be used.

Recently, a more consistent NLO formulation of heavy flavour dynamics within the perturbative-QCD (pQCD) framework has been given, in Refs. [33, 41, 40]. The new treatment encompasses both the 'flavour creation' and 'flavour excitation' mechanisms and is valid from the heavy quark threshold up to the high energy regime. It makes use of a finite value of m_b throughout the all μ range. It reduces to the two above approaches in the appropriate limits: i.e., to the TFN scenario when $\mu \sim m_q$ and to the FFN one

[8] We have verified that differences in the results similar to those obtained in case of process (4) also occur for the complete tree-level reactions (5)–(7).

if $\mu \gg m_q$ (where $q = c, b$)[9]. Although the three formulations in Refs. [33, 41, 40] are slightly different, their approach is basically the same. Furthermore, based on the 'improved theory' for heavy quark dynamics, global analyses and new PDF packages have been made available, such as the MRRS(1,2,3) [33] and CTEQ(4HQ) [37] sets. In many respects, these sets represent the most advanced ones to date in describing the dynamics of heavy flavours.

Preliminary comparisons between the various 'heavy quark sets' and old sets have been performed in Refs. [41, 40, 42], though results are not conclusive yet, since similarly fitted parton distributions in the various schemes are not available in the literature at the moment, to allow for a consistent study [37]. Being such a comparison beyond the scope of this paper, we confine ourselves to the computation of some relevant rates of process (4) with the mentioned NLO sets. In this respect, some peculiar differences between the various PDFs should be recalled. For a start, the choice of the threshold μ_b can vary, being in some instances set at $\mu_b^2 = m_b^2$ (see, e.g., Ref. [29]) and in other cases at $\mu_b^2 = 4m_b^2$ (see, e.g., Ref. [35]). Furthermore, it is evident that the actual value of m_b can have a strong impact on the $g \to b\bar{b}$ dynamics. We will match our input parameter m_b to the default values of the various PDFs. We shall use m_b=0 in the 'massless' PDFs (all sets apart from MRRS(1,2,3) and CTEQ(4HQ)), whereas in the 'massive' ones we adopt a finite value: i.e., 4.3 GeV for MRRS(1,2,3)[10] and 5.0 GeV for CTEQ(4HQ). Finally, one should remember that also the value of α_s associated with each parton set represents in principle a residual source of error in the predictions of the different PDFs [31]. However, the value adopted in each set is chosen to match the data during the extraction, so that we do not expect α_s to be a significant source of uncertainty.

For the top mass we have taken (unless otherwise stated) $m_t = 175$ GeV [2], whereas for the width Γ_t we have used the tree-level expression [43]. Leptons and u, d, s (and c as well) quarks were considered as massless in processes (5)–(7). For simplicity, we set the Cabibbo-Kobayashi-Maskawa (CKM) mixing matrix element of the top-bottom coupling equal to one, the Standard Model prediction at the 90% confidence level [44] being $0.9989 \leq |V_{tb}| \leq 0.9993$. For the gauge boson masses and widths we used $M_Z = 91.19$ GeV, $\Gamma_Z = 2.50$ GeV, $M_{W^\pm} = 80.23$ GeV and $\Gamma_{W^\pm} = 2.08$ GeV. The electromagnetic coupling constant and the weak mixing angle are $\alpha_{em} = 1/128$ and $\sin^2\theta_W = 0.2320$, respectively.

The Higgs boson of the Standard Model enters directly in the diagrams of Figures 1b (graphs 3 and 16) and c (graph 7), when the bottom quark mass is retained in the fermion-fermion-scalar vertex (as the procedure is gauge invariant, a $g_{b\bar{b}H} \neq 0$ Yukawa coupling has been maintained in the corresponding Feynman rule even when the value $m_b = 0$ has been adopted elsewhere in the matrix elements). As default value for the scalar mass we used $M_H = 150$ GeV, consistent with the best χ^2 fit as obtained from the analysis of the LEP and SLC high precision EW data: i.e., $M_H = 115^{+116}_{-66}$ GeV [45]. However, since the constraints on the Higgs mass are rather weak (a lower bound of about 70 GeV from direct searches and a 95% confidence level upper limit of 420 GeV

[9] As this new approach effectively interpolates between the preceeding two, it is often referred to as the Variable-Flavour-Number (VFN) scheme.

[10] Note that the charm mass m_c in the three above packages has been set equal to 1.35, 1.50 and 1.2 GeV, respectively: this is however a 'dummy' value in the production process (4).

from the data mentioned) we studied the M_H dependence of the EW contributions in processes (5)–(6) and (8)–(9), and found it negligible (note that the Higgs boson is always produced via non-resonant channels in those reactions). This is also true for the $2b$ process, after the implementation of the selection cuts (see below).

Finally, as total CM energy $\sqrt{s}_{ep}$ of the colliding positron-proton beams we have adopted values in the range between 300 GeV (i.e., around the HERA value) and 2 TeV. However, we focused our attention mainly to the case of a possible LEP2⊕LHC accelerator, using a 100 GeV positron beam from LEP2 and a 7 TeV proton one from the LHC, yielding the value $\sqrt{s}_{ep} \approx 1.7$ TeV in the CM frame of the colliding particles.

3. Results

As emphasised in Section 1, we generate the single top quark in the final state by means of the matrix element for e^+b fusion (4) convoluted with b structure functions rather than producing the initial b quark via an exact $g \to b\bar{b}$ splitting folded with a gluon density. However, to investigate the differences between the two procedures, we show in Figure 2 the total cross section of the signal process (4) plotted against the CM energy of the ep system along with the yield of reaction (1) (the latter including top decays and finite width effects on the same footing as the former)[11]. For reference, the PDFs used here are the CTEQ(4HQ) ones, in order to test the performances of the recently developed theory for heavy flavours.

Care must be taken when comparing processes (1) and (4) with respect to each other. In fact, one should recall that the corresponding rates are strongly dependent on the (factorisation) scale μ. In general, the $W^\pm g$ fusion cross section decreases sharply as the scale increases, whereas that of e^+b events goes up mildly as μ gets larger (see Ref. [27] for a dedicated study in the case of $p\bar{p}$ collisions at the Tevatron). Although at LO there is no privileged choice for μ, Ref. [19] has shown that the most appropriate scale at the exact NLO (when both processes (1) and (4) need to be calculated) in the b distribution function is $\mu^2 \approx Q^2 + m_t^2$, where $Q^2 \equiv -q^2$ (q being the four-momentum of the incoming virtual $W^\pm$ boson). Therefore, we have adopted this value in producing Figure 2 (also as argument of the strong coupling constant), whereas in all other cases we will maintain the LO 'running' choice $\mu = \sqrt{\hat{s}}$. This has been done for two reasons. First, we have verified that for $\mu \gtrsim \sqrt{\hat{s}}_{min} \approx m_t$ the rates of process (4) are rather stable, showing variations below 6-7%. Second, this choice of the scale allows one to consistently incorporate the non-resonant diagrams along with the top ones when calculating the cross sections of the complete processes (5)–(7).

From Figure 2, it is clear that, apart from the different normalisation, the threshold behaviour in processes (1) and (4) is substantially similar as a function of the total CM energy. Though, the ratio between the two series of curves is approximately 4.7-5.3 at 300 GeV and it decreases with increasing energy, stabilising at 1.3 TeV or so around 1.7–1.8. We trace back the behaviour of the ratio at high energies as due to

[11]Note that in order to obtain a gauge invariant cross section for process (1) in presence of a finite value of Γ_t we need to consider a set of three diagrams. That is, the two with resonant top production (i.e., those in Figure 1a with the additional decay $t \to bW^+ \to bf\bar{f}'$) and a third one in which the $W^+ \to f\bar{f}'$ current is attached to the off-shell fermion propagator in one of the graphs of Figure 1a.

the fact that the terms $\alpha_s(\mu^2)\log(\mu^2/m_b^2)$ become constant because of large logarithms cancelling each other ($\alpha_s(\mu^2)$ is in fact proportional to $1/\log(\mu^2/\Lambda^2_{\rm QCD})$). In contrast, at lower energies (well below the TeV scale) this is no longer the case and, in addition, graph 2 of Figure 1a becomes strongly suppressed, thus explaining the increase of the observed ratio. The value of the latter between the two cross sections when $\sqrt{s_{ep}} \gtrsim 1.3$ TeV can be understood in terms of the large logarithms entering in the resummation of the b structure function, which tend to enhance the b induced process with respect to the g one. For example, for $\mu^2 = m_t^2$, with $m_t = 170(175)[180]$ GeV, one gets the 'leading logs' $L = \alpha_s(\mu^2)\log(\mu^2/m_b^2) \approx 0.75(0.76)[0.76]$. Such differences between b and $g \to b\bar{b}$ induced processes at the TeV scale are not unusual in literature, see, e.g., Refs. [27, 46] (though, for the case of hadron-hadron collisions at the TeV scale). Note that we obtain the same pattern also for the case of on-shell top production, when no decay of the top quark is implemented.

Before proceeding, we should in fact mention that we have studied the size of the differences between the total rates of the two processes as obtained, on the one hand, by using a finite width and implementing the decay currents and, on the other hand, by keeping the top on-shell. In general, they are at the level of few percent (the on-shell rates being larger). For example, for the $b(g)$ induced process they vary between 2(1)% to 4(5)% when $m_t = 175$ GeV. In fact, rates are rather insensitive to the value of the top mass.

From Figure 2, we further note that although the cross section for process (4) is small at existing collider energies ($\sqrt{s_{ep}} \approx 300$ GeV at DESY leads to a total cross section of less than 1 fb, which is negligible given the current integrated luminosity of about 20 pb^{-1} [47] at each of the two experiments), it increases steeply near the TeV scale. At the LEP2$\oplus$LHC scale it is easily observable at the 'conservative' luminosity of 100 pb^{-1} [48]. There is however a sizeable dependence on the top quark mass, especially at low energies: the cross section being smaller for a phase space suppressed by a higher mass. (All our results hereafter assume the central value of 175 GeV.)

Table I shows the cross section of the signal process (4) evaluated at the LEP2$\oplus$LHC energy, for the discussed twenty-six different sets of structure functions. In the top line, separated from the rest, we report the value obtained for the LO set CTEQ(4L). As already mentioned, this is the most 'consistent' result, as our ME for the hard-scattering process (4) has been computed at LO. However, as explained in the previous Section, we will resort to the 25 NLO PDFs to estimate the error due to the b quark distribution. The PDF dependence is found to be approximately 20-25%, with the maximum value of the total cross section differing from the minimum value by 854 fb. We believe such theoretical uncertainty to be already at the present time a reasonably small error so to motivate further and more detailed simulation studies (including hadronisation, detector effects, reducible background [16, 49]) of single top phenomenology. To appreciate this we note that the result obtained by adopting the old LO set EHLQ1 [50] (i.e., the one used in Ref. [16]) differs by that produced by CTEQ(4L) in Table I by more than 50% !

As a further example, we present the Bjorken x and the Q dependence of the cross section of process (4) for a selection of NLO PDFs, in Figures 3a and 3b (respectively). In particular, we have included results for some older, MRS(R1) and CTEQ(3M), and some newer, MRRS(1) and CTEQ(4HQ), sets, as representative of the two approaches

MRS and CTEQ, each of the pair being fitted to a similar set of experimental data so to allow for a more consistent comparison. Note that the normalisations of the curves are to unity, in order to enlighten the differential behaviours of these quantities, in addition to their effects on the total rates (as was done in Table I). The clear message from Figures 3a and 3b is that the differences between the two pairs of sets are very small (as can be appreciated in detail in the central inserts), typically a few percent over all the available kinematic range in x and Q. Although we do not show the corresponding curves, we have verified that such considerations also apply to the other PDFs considered here. Thus, also at differential level the theoretical error on the rates of process (4) due to the PDFs is well under control already at present.

Though it is beyond the scope of this study to trace back whether the differences in Table I (and Figures 3a–b) among the various sets are due to the gluon structure function or to the $g \to b\bar{b}$ splitting (which onsets the b structure function), it is worth mentioning that it could well be that by the time a future ep collider will be running the uncertainties on the former will be so under control that one might attempt to distinguish between different dynamics proposed for the latter. In this respect, it would be interesting to assess whether the differences between MRRS(1) (dashed line) and CTEQ(4HQ) (dot-dashed line) among each other and with respect to MRS(R1) and CTEQ(3M), respectively, in Table I and in Figures 3a and 3b are genuinely due to the dedicated treatment of the heavy quark PDFs or not [51]. Clearly, this will require a tight control on all sources of experimental error, in particular of the actual value of the b-tagging efficiency and of the hadronisation process of the quarks at the TeV scale.

Figure 4 shows the differential distributions interesting for the final state phenomenology of the single-top signal (4) in its hadronic (ff' = jet-jet) and leptonic ($ff' = \ell\nu_\ell$) channels. Those in combined jet masses are sharply peaked at the top and $W^\pm$ masses well above the irreducible noise, indicating that for the hadronic case the jet masses can be used to clearly identify the top decays. This feature is convenient both for the elimination of top events from any other hadronic three-jet processes to which the former may act as a background, and for the elucidation of the top quark physics at ep colliders in, for example, probing the b quark distribution function. The spectra in transverse momenta p_T show that neither cuts in p_T nor cuts in p_T^{miss} affect the total cross section dramatically, whereas that of ΔR, the azimuthal-pseudorapidity separation defined by $\Delta R = \sqrt{(\Delta\phi)^2 + (\Delta\eta)^2}$ (where ϕ is the azimuthal angle and η the pseudorapidity) indicates that the requirement of resolving the hadronic jets (or the requirement of an isolated lepton in the leptonic case) severely reduces the event rate. The majority of events are found within $\Delta R \lesssim 1.5$, which is about 90 degrees in the azimuthal angle. This is because the visible jets and the lepton come from the energetic top quark. Thus, at lower energies the azimuthal-pseudorapidity spread in the top quark decay products will be larger and hence the requirement of such jet/lepton isolation not so stringent. The distribution of the missing transverse momentum in the leptonic case, and more specifically the electronic case, is small at low missing p_T and indicates that only a small proportion of the events will emulate neutral current events of the form $ep \to eX$. However, those which do will form a potentially dangerous background to high Q^2 neutral current events, as the low ΔR mentioned above will concentrate the electrons to the high Q^2 region.

Table II and Figure 5 show the total cross section after the acceptance cuts. The following LHC-like constraints were implemented (see [16] for alternative selection strategies): for the leptonic channel, $p_T^{\ell^+}, p_T^b > 20$ GeV, $p_T^{miss} > 10$ GeV and $\Delta R_{\ell^+,b} > 0.7$; for the hadronic channel, $p_T^{j,j'}, p_T^b > 20$ GeV, $p_T^{miss} > 10$ GeV and $\Delta R_{j,j',b} > 0.7$. We have not introduced any cuts on pseudorapidity, as the particles were found to be all concentrated in the narrow $|\eta| < 2.5$ region even before any selection in p_T was made.

Table II summarises the event rates for all channels at three different CM energies. The numbers in square brackets are the cross sections of processes (8) and (9). These are additional backgrounds when bottom quark charge tagging is unavailable. Since these effectively only differ from processes (5) and (6) in their non-resonant top quark production, they can be taken as a measure of the magnitude of the irreducible background. As can be noticed, such background effects are small. We see that the hadronic cross section is higher at lower energy since, as discussed above, the acceptance cut in ΔR affects the rates less at smaller values of $\sqrt{s_{ep}}$, thus compensating for the reduced total cross section shown in Figure 2. From Figure 5 we see that background effects do not spoil the sharp resonances in combined jet masses even after the acceptance cuts. We particularly stress that the QCD background is negligible: luckily enough, as it curiously peaks around the $M_{W^\pm}$ value in the di-jet mass distribution. It can also be noted that the cut in ΔR, the jet separation, of 0.7 is a conservative choice and, as can be deduced from the distribution in ΔR in Figure 4, so that the rates should be expected much higher for looser constraints, especially for the hadronic channel when three separate cuts in ΔR need to be made to resolve the three jets completely. Finally, given the optimistic vertex tagging performances foreseen for the LHC detectors [9], we would expect that only a small fraction of the event rates given in Table II will be lost in the actual analyses. In fact, we believe that the original capabilities of the LHC μ-vertex devices will be maintained while running the CERN machine in the proposed ep mode.

4. Summary and conclusions

The single top quark production from initial state bottom sea quark at future ep colliders was studied, mainly focusing our attention to the case of the proposed LEP2$\oplus$LHC accelerator with the positron (electron) beam energy of 100 GeV and the proton one of 7 TeV. The total cross section was found to be about 4 pb at this energy. The uncertainty due to the structure functions was quantified to be rather small already at the present time, around 20-25%, and is expected to diminish significantly before new ep machines will enter into operation. Furthermore, based on such a consideration, some optimistic prospects about the possibility of exploiting single top phenomenology in order to study the $g \to b\bar{b}$ dynamics inside the proton were given. Both the leptonic and hadronic decay channels of the top quark were studied, in presence of the corresponding irreducible backgrounds, which have been computed here for the first time. In the hadronic case, distributions in the reconstructed top quark and $W^\pm$ boson masses were found to be sharply peaked above the irreducible noise, so to allow for a prompt recognition of single top events. In both channels the cross section for the background was found to be small compared with the signal events. The residual dependence of the latter on the top quark mass was evaluated in several instances. Finally, the formula for the matrix element squared of single top production, including top width effects and all the dynamic correlations between the top decay products, was presented in order to aid future, more detailed, experimental simulations. The complete numerical programs, evaluating irreducible background effects as well, have been especially optimised in view of high statistic Monte Carlo simulations and are available from the authors upon request.

5. Acknowledgements

SM is grateful to the UK PPARC and KO to Trinity College and the Committee of Vice-Chancellors and Principals of the Universities of the United Kingdom for financial support. SM also acknowledges the kind hospitality of the Theoretical Physics Groups at Fermilab (USA) and Lund (Sweden), where part of this work was carried out. Finally, the research performed in Lund by SM has been partially supported by the Italian Institute of Culture 'C.M. Lerici' under the grant Prot. I/B1 690, 1997.

References

[1] CDF Collaboration, Phys. Rev. Lett. **74**, 2626 (1995); D0 Collaboration, Phys. Rev. Lett. **74**, 2632 (1995).

[2] See, e.g.:
R. Raja, Talk presented at the XXXII Rencontres de Moriond on Electroweak Interactions and Unified Theories, Les Arcs, Savoie, France, March 15–22, 1997;
M. Cobal, presented at the *Fifth Topical Seminar on the Irresistible Rise of the Standard Model*, San Miniato, Tuscany, Italy, April 21–25, 1997.

[3] Proceedings of the ECFA Large Hadron Collider Workshop, Aachen, Germany, edited by G. Jarlskog and D. Rein (CERN Report No. 90–10, ECFA Report No. 90–133, Geneva, Switzerland, 1990).

[4] R. Rückl, in [3].

[5] A.C. Bawa and M. Krawczyk, in Proceedings of the 1991 HERA Physics Workshop, Hamburg, 1992.

[6] See, e.g.:
Proceedings of the Workshop 'Future Physics at HERA', eds. G. Ingelman, A. De Roeck and R. Klanner (DESY, Hamburg, 1995/96).

[7] G. Grindhammer, D. Haidt, J. Ohnemus, J. Vermaseren and D. Zeppenfeld, in [3].

[8] P. Igo-Kemenes, talk given at the *Phenomenology Workshop on LEP2 Physics,* Oxford, UK, 14–18 April 1997.

[9] CMS Technical Proposal, CERN/LHC/94–43 LHCC/P1 (December 1994); ATLAS Technical Proposal, CERN/LHC/94–43 LHCC/P2 (December 1994).

[10] J.F. Gunion, A. Stange, S. Willenbrock, in *Electroweak Symmetry Breaking and New Physics at the TeV scale* (World Scientific, Singapore, 1996).

[11] J.L. Diaz-Cruz and O.A. Sampayo, Barcelona Autonoma University Report No. UAB–FT–286–92, 1992 (unpublished).

[12] S. Moretti and K. Odagiri, in preparation.

[13] Proceedings of the Workshop "*e^+e^- Collisions at 500 GeV. The Physics Potential* ", Munich, Annecy, Hamburg, 3–4 February 1991, ed. P.M. Zerwas, DESY 92–123A/B, August 1992, DESY 93–123C, December 1993.

[14] G. Abu Leil and S. Moretti, Phys. Rev. **D53**, 163 & 178 (1996); K. Cheung, Phys. Lett. **B319**, 244 (1993).

[15] Proceedings of the International Workshop on Linac-Ring Type ep and Gamma-p Colliders, Ankara, Turkey, 9–11 April 1997, to be published in the Turkish Journal of Physics.

[16] A. Ali, F. Barreiro, J.F. de Trocóniz, G.A. Schuler and J.J. van der Bij, in [3].

[17] J. van der Bij and U. Baur, Nucl. Phys. **B304**, 451 (1988); G. Schuler, Nucl. Phys. **B229**, 21 (1988); J. van der Bij and G. J. van Oldenborgh, Z. Phys. **C51**, 477 (1991).

[18] F. Olness and W.-K. Tung, Nucl. Phys. **B308**, 813 (1988); R. Barnett, H. Haber, and D. Soper, Nucl. Phys. **B306**, 697 (1988); M. Aivazis, J. Collins, F. Olness, and W.-K. Tung, Phys. Rev. **D50**, 3102 (1994).

[19] T. Stelzer, Z. Sullivan and S. Willenbrock, hep-ph/9705398.

[20] G. Bordes and B. van Eijk, Nucl. Phys. **B435**, 23 (1995).

[21] T. Stelzer and W.F. Long, Comp. Phys. Comm. **81**, 357 (1994).

[22] H. Murayama, I. Watanabe and K. Hagiwara, HELAS: HELicity Amplitude Subroutines for Feynman Diagram Evaluations, *KEK Report* 91–11, January 1992.

[23] C. Becchi, A. Rouet and R. Stora, Ann. Phys. **98**, 287 (1976); G.J. Gounaris, R. Kogerler and H. Neufeld, Phys. Rev. **D34**, 3257 (1986).

[24] G.P. Lepage, Jour. Comp. Phys. **27**, 192 (1978).

[25] R.K. Ellis and S. Parke, Phys. Rev. **D46**, 3785 (1992).

[26] V.N. Gribov and L.N. Lipatov, Sov. J. Nucl. Phys. **15**, 438 (1972); ibidem **15**, 675 (1972); Yu.L. Dokshitzer, Sov. Phys. JETP **46**, 641 (1977); G. Altarelli and G. Parisi, Nucl. Phys. **B126**, 298 (1977).

[27] A.P. Heinson, A.S. Belyaev and E.E. Boos, hep-ph/9612424.

[28] A.D. Martin, R.G. Roberts and W.J. Stirling, Phys. Rev. **D50**, 6734 (1994); A.D. Martin, R.G. Roberts and W.J. Stirling, Phys. Rev. **D51**, 4756 (1995).

[29] A.D. Martin, R.G. Roberts and W.J. Stirling, Phys. Lett. **B354**, 155 (1995).

[30] A.D. Martin, R.G. Roberts and W.J. Stirling, Phys. Lett. **B387**, 419 (1996).

[31] A.D. Martin, R.G. Roberts and W.J. Stirling, Phys. Lett. **B356**, 89 (1995).

[32] E.W.N. Glover, A.D. Martin, R.G. Roberts and W.J. Stirling, Phys. Lett. **B381**, 353 (1996).

[33] A.D. Martin, R.G. Roberts, M.G. Ryskin and W.J. Stirling, preprint DTP/96/102, December 1996, hep-ph/9612449.

[34] W.-K. Tung, Proceedings of the International Workshop on Deep Inelastic Scattering and Related Subjects, Eilat, Israel, 1994, ed. A. Levy (World Scientific, Singapore, 1995).

[35] H.L. Lai, J. Botts, J. Huston, J.G. Morfin, J.F. Owens, J. Qiu, W.K. Tung and H. Weerts, Phys. Rev. **D51**, 4763 (1995).

[36] H.L. Lai, J. Huston, S. Kuhlmann, F. Olness, J.F. Owens, D. Soper, W.K. Tung and H. Weerts, Phys. Rev. **D55**, 1280 (1997).

[37] H.L. Lai and W.K. Tung, Z. Phys. **C74**, 463 (1997).

[38] M. Gluck, E. Hoffmann and E. Reya, Z. Phys. **C13**, 119 (1982);
S. Kretzer, E. Reya and M. Stratmann, Phys. Lett. **B348**, 628 (1995).

[39] M. Glück, E. Reya and A. Vogt, Z. Phys. **C67**, 433 (1995).

[40] M. Buza, Y. Matiounine, J. Smith and W.L. van Neerven, preprint NIKHEF-96-027, ITP-SB-96-66, DESY-96-258, INLO-PUB-22-96, December 1996, hep-ph/9612398; preprint NIKHEF-97-026, ITP-SB-97-35, DESY-97-124, INLO-PUB-6-97, July 1997, hep-ph/9707263.

[41] M.A.G. Aivazis, F.I. Olness and W.K. Tung, Phys. Rev. **D50**, 3085 (1994); Phys. Rev. **D50**, 3102 (1994).

[42] V. Barone and M. Genovese, *Phys. Lett.* **B379**, 233 (1996);
V. Barone, U. d'Alesio and M. Genovese, hep-ph/9610211.

[43] J.H. Kühn, Act. Phys. Pol. **B12**, 347 (1981); J.H. Kühn, Act. Phys. Austr. Suppl. **XXIV**, 203 (1982).

[44] See, e.g.:
Particle Data Group, Phys. Rev. **D54**, 1 (1996) (and references therein).

[45] The LEP Electroweak Working Group and the SLD Heavy Flavor Group, preprint LEPEWWG/97–02, ALEPH 97–085 PHYSIC 97–075, DELPHI 97–141 PHYS 726, L3 Note 2153, OPAL Technical Note TN 504, SLD Physics Note 63, 18 August 1997.

[46] W.J. Stirling and D.J. Summers, Phys. Lett. **B283**, 411 (1992); A. Ballestrero and E. Maina, Phys. Lett. **B299**, 312 (1993).

[47] H1 Collaboration, Z. Phys. **C74**, 191 (1997); ZEUS Collaboration, Z. Phys. **C74**, 207 (1997).

[48] J. Feltesse, in [3].

[49] G. Ingelman, J. Rathsman and G. A. Schuler, Comput. Phys. Commun. **101**, 135 (1997) (and references therein).

[50] E. Eichten, I. Hinchliffe, K. Lane and C. Quigg, Rev. Mod. Phys. **56**, 579 (1984); Erratum, ibidem **58**, 1065 (1986).

[51] F.I. Olness and R.J. Scalise, preprint CTEQ-708, SMU-HEP-9709, July 1997, hep-ph/9707459.

Table Captions

[I] Total cross sections (hadronic and leptonic) for process (4) at LEP2⊕LHC energies for twenty-six different sets of structure functions. Errors are as given by VEGAS (the same statistics were used for the `NCALL` and `ITMX` parameters) [24].

[II] Total cross sections (hadronic and leptonic, including irreducible background effects) for processes (5)–(7) at the LEP2⊕LHC collider. The structure function set CTEQ(4L) was used. Errors are as given by VEGAS [24]. The following acceptance cuts were implemented: (i) $p_T^{\ell^+}, p_T^b > 20$ GeV, $p_T^{miss} > 10$ GeV and $\Delta R_{\ell^+,b} > 0.7$ (leptonic channel); (ii) $p_T^{j,j'}, p_T^b > 20$ GeV, $p_T^{miss} > 10$ GeV and $\Delta R_{j,j',b} > 0.7$ (hadronic channel). In the squared brackets of the first two columns we report the rates of the charge conjugates (8)–(9) of processes (5)–(6), for which the resonant top production do not occur. The rates of the charge conjugate of process (7) are the same as those in third column.

Figure Captions

[1] Lowest order Feynman diagrams describing processes (1), (5), (6) and (7), corresponding to sets (**a**), (**b**), (**c**) and (**d**), respectively. Only the cases $\ell^+\nu_\ell = e^+\nu_e$ and $jj' = u\bar{d}$ are shown are shown for processes (5)–(7), whereas in reaction (1) the top is considered on-shell. The package MadGraph [21] was used to produce the PostScript codes. In (**c**) 'A' represents the photon. The dashed lines in (**b**) and (**c**) represent the SM Higgs boson and the curly lines in (**d**) the gluon. The number of diagrams in (**b**) reduces to 10 for the cases $\ell^+\nu_\ell = \mu^+\nu_\mu$ and $\tau^+\nu_\tau$, when diagrams 1, 2, 3, 5, 6, 7, 8, 12, 13, 20 and 21 do not contribute.

[2] The total cross section (hadronic and leptonic channels) for processes (4) (upper lines) and (1) (lower lines) for 300 GeV $\leq \sqrt{s}_{ep} \leq$ 2 TeV, with three different values for the top quark mass: m_t = 170 GeV (continuous line), m_t = 175 GeV (dashed line) and m_t = 180 GeV (dotted line). The structure function set CTEQ(4L) was used.

[3] Differential distributions in (**a**) x and (**b**) Q for events of the type (4) at the LEP2⊕LHC collider for three representative sets of structure functions: MRS(R1) (solid), MRRS(1) (dashed), CTEQ(3M) (dotted) and CTEQ(4HQ) (dot-dashed). In the central inserts, the spectra are magnified around their maximum values. Normalisations are to unity.

[4] Differential distributions (hadronic and leptonic channels) for the signal process (4) at the LEP2⊕LHC CM energy and m_t = 175 GeV in the following variables (clockwise). 1. $M_{\rm jets}$, the invariant mass of the two- (solid) and three-jet (dashed) systems in hadronic decays. 2. p_T, the transverse momenta of the lepton/jets (solid) in leptonic/hadronic decays, of the bottom quark (dashed) in both channels, and of the missing particles in leptonic (dotted) and hadronic (dot-dashed) decays. 3. ΔR, the azimuthal-pseudorapidity separation of the pairs lepton/jets-bottom quarks (solid) in leptonic/hadronic decays. The normalisation is to unity. The structure function set CTEQ(4L) was used. In the case of the hadronic decays we have considered only one of the two light quark jets, their distributions in the above variables being very similar.

[5] Differential distributions in $M_{\rm jets}$ (hadronic channel only) for processes (6) (left) and (7) (right) at the LEP2⊕LHC CM energy and m_t = 175 GeV. $M_{\rm jets}$ signifies the invariant mass of the two- (solid) and three-jet (dashed) systems in hadronic decays. The normalisations are to the total cross sections. The structure function set CTEQ(4L) was used. Bins are 2 GeV wide. The following acceptance cuts were implemented: $p_T^{j,j'}, p_T^b > 20$ GeV, $p_T^{miss} > 10$ GeV and $\Delta R_{j,j',b} > 0.7$ (hadronic channel).

single-top	
PDFs	σ_t (fb)
CTEQ(4L)	3551 ± 13
MRS(A)	3760 ± 15
MRS(A')	3680 ± 14
MRS(G)	3565 ± 14
MRS(J)	3811 ± 15
MRS(J')	4081 ± 16
MRS(R1)	3476 ± 14
MRS(R2)	3740 ± 14
MRS(R3)	3547 ± 13
MRS(R4)	3786 ± 15
MRS(105)	3334 ± 13
MRS(110)	3556 ± 13
MRS(115)	3529 ± 14
MRS(120)	3824 ± 15
MRS(125)	3844 ± 15
MRS(130)	3913 ± 15
MRRS(1)	4063 ± 16
MRRS(2)	4070 ± 15
MRRS(3)	4055 ± 16
CTEQ(2M)	3852 ± 16
CTEQ(2MS)	3729 ± 15
CTEQ(2MF)	3879 ± 15
CTEQ(2ML)	4188 ± 16
CTEQ(3M)	4158 ± 16
CTEQ(4M)	4065 ± 15
CTEQ(4HQ)	4006 ± 15
no acceptance cuts	
LEP2$\oplus$LHC	

Table I

σ_{tot} (fb)			
$\sqrt{s}_{ep}$ (TeV)	leptonic	hadronic (EW)	hadronic (QCD)
1.0	$193.8 \pm 2.7[2.077 \pm 0.024]$	$226.3 \pm 2.1[1.862 \pm 0.014]$	3.436 ± 0.011
1.3	$331.6 \pm 9.3[3.879 \pm 0.071]$	$210.5 \pm 3.3[2.591 \pm 0.059]$	4.904 ± 0.017
1.7	$514. \pm 13.[6.959 \pm 0.081]$	$124.5 \pm 5.4[3.250 \pm 0.076]$	6.505 ± 0.021
after acceptance cuts			
CTEQ(4L)			

Table II

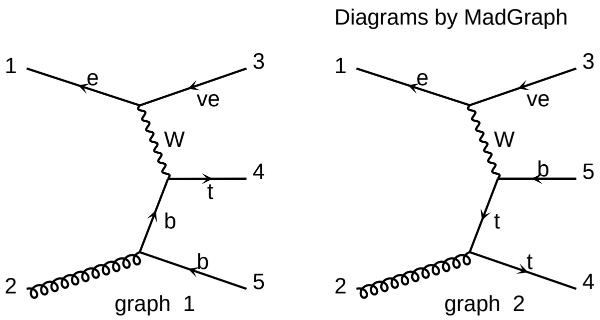
Diagrams by MadGraph
1
e
3
ve
W
4
t
b
2
b
5
graph 1
1
e
3
ve
W
b
5
t
2
t
4
graph 2

Fig. 1a

Diagrams by MadGraph

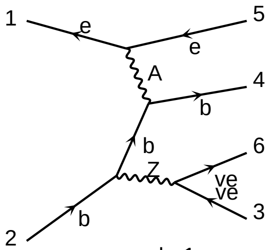

graph 1

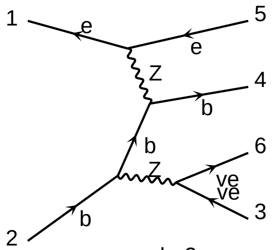

graph 2

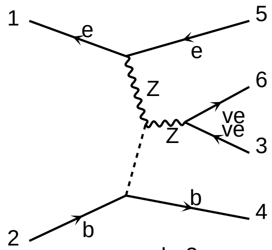

graph 3

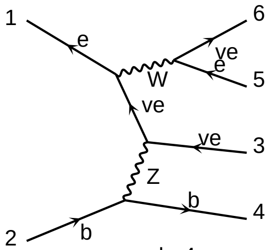

graph 4

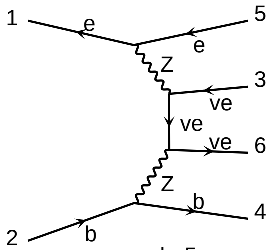

graph 5

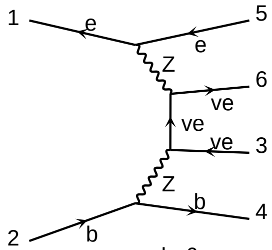

graph 6

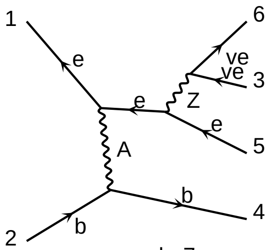

graph 7

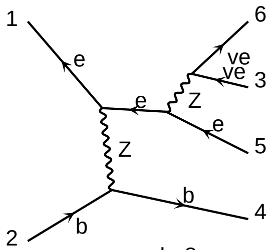

graph 8

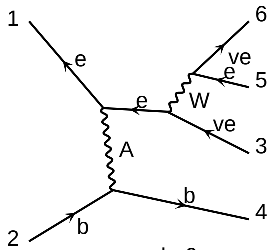

graph 9

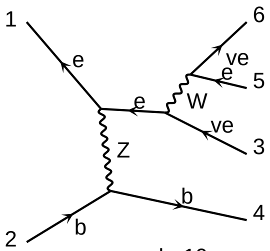

graph 10

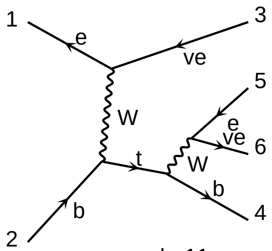

graph 11

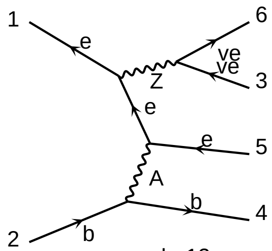

graph 12

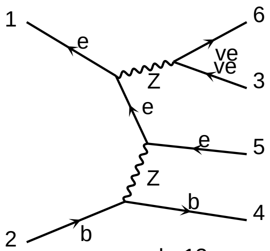

graph 13

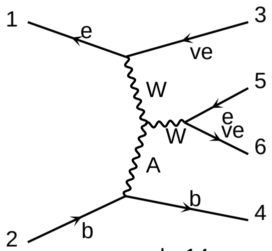

graph 14

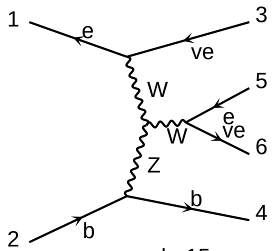

graph 15

continues

Diagrams by MadGraph

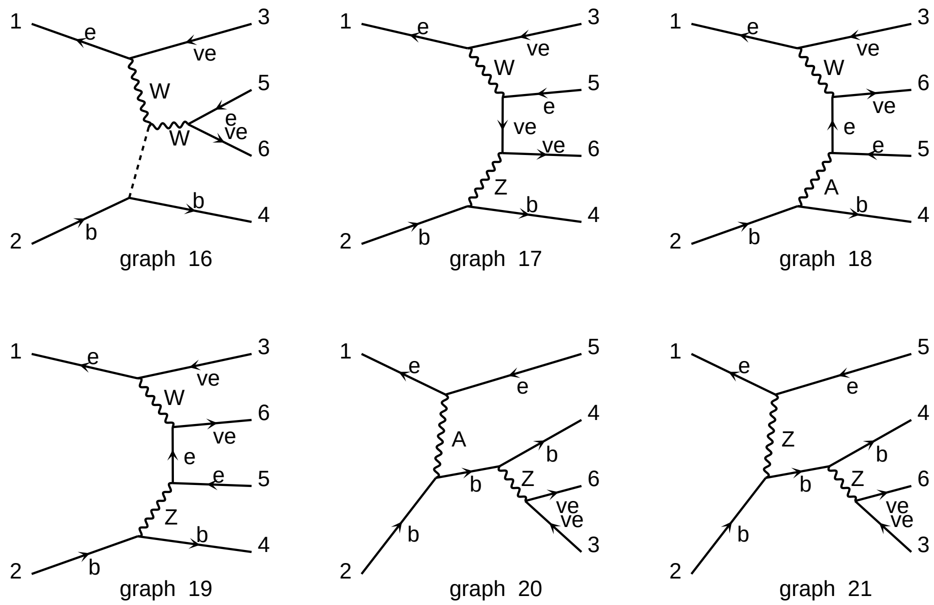

Fig. 1b

Diagrams by MadGraph

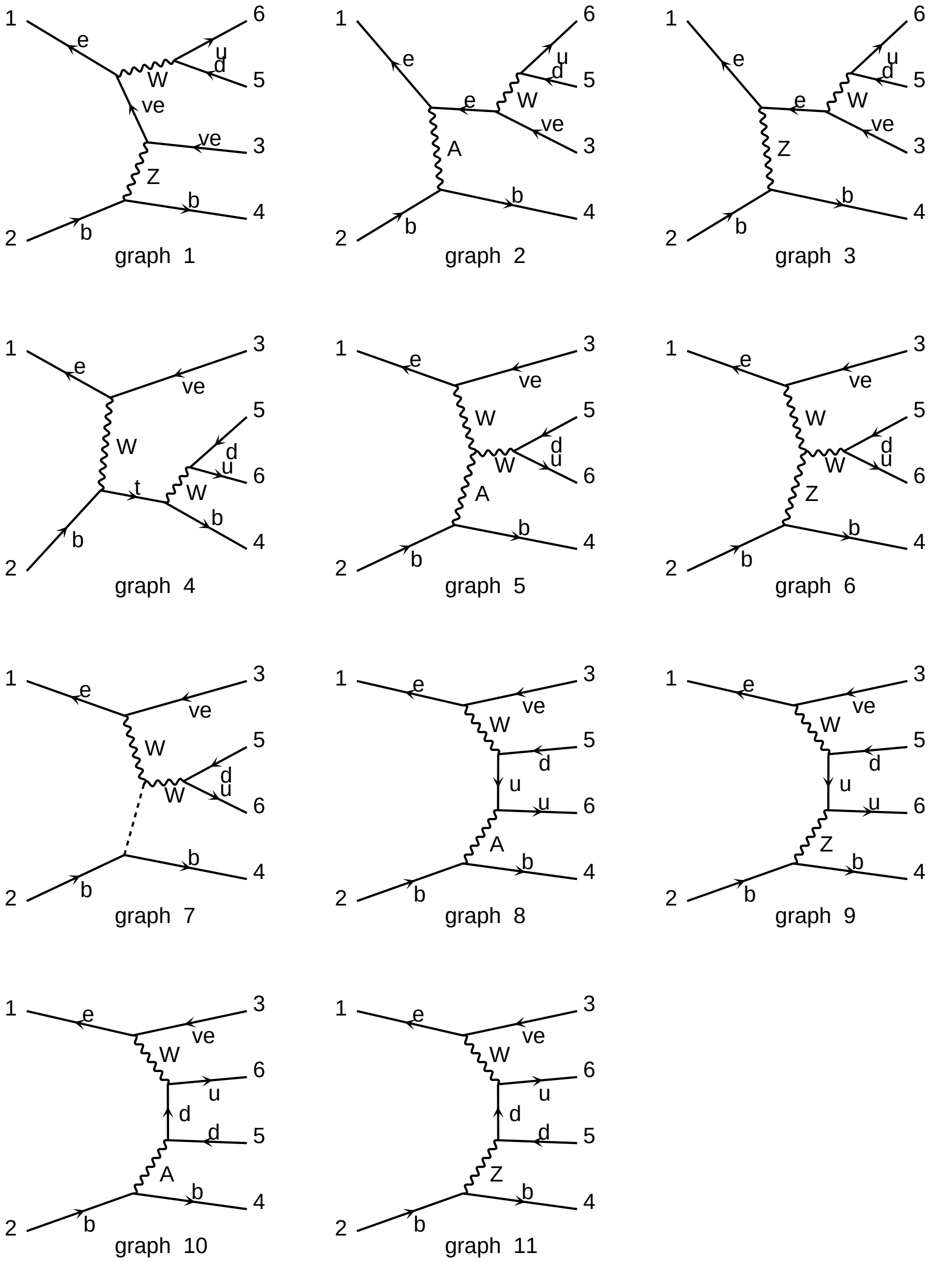

Fig. 1c

Diagrams by MadGraph

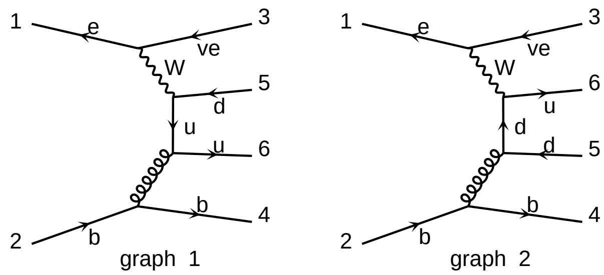

Fig. 1d

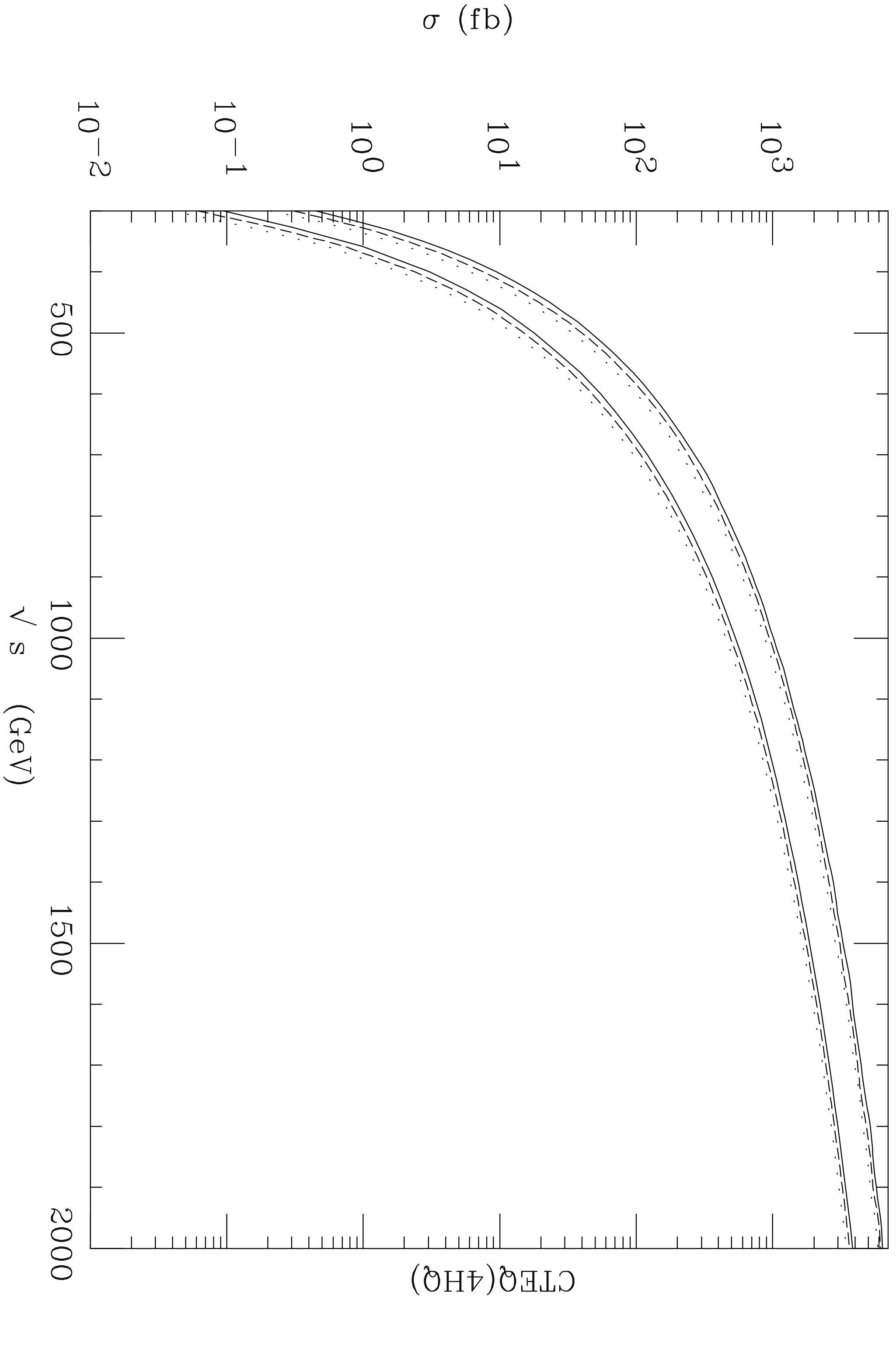

σ (fb)
10^{-2}
10^{-1}
10^{0}
10^{1}
10^{2}
10^{3}
500
1000
1500
2000
$\sqrt{s}$ (GeV)
CTEQ(4HQ)

Fig. 2

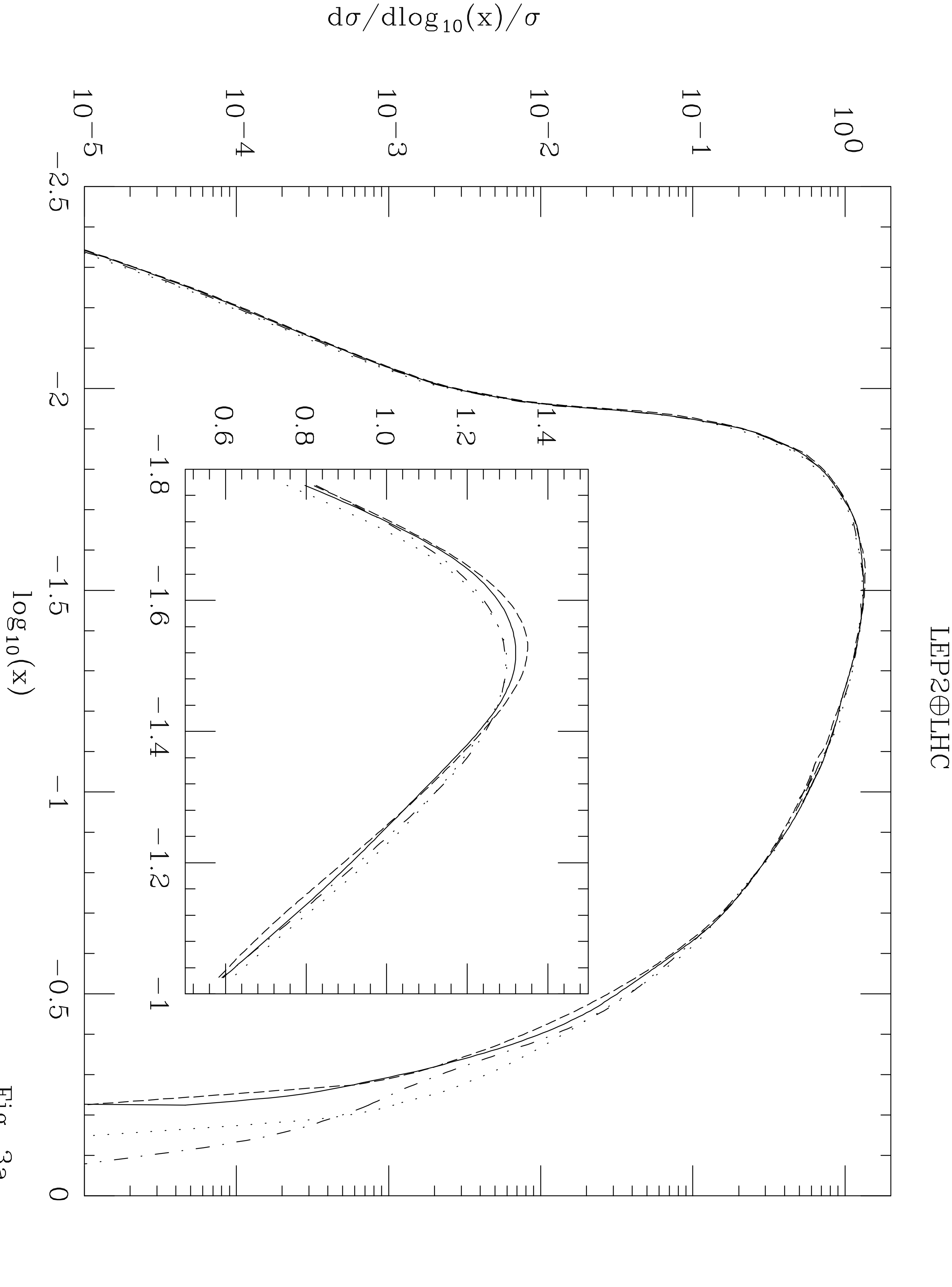

LEP2⊕LHC
$d\sigma/d\log_{10}(x)/\sigma$
$\log_{10}(x)$
10^{0}
10^{-1}
10^{-2}
10^{-3}
10^{-4}
10^{-5}
−2.5
−2
−1.5
−1
−0.5
0
1.4
1.2
1.0
0.8
0.6
−1.8
−1.6
−1.4
−1.2
−1

Fig. 3a

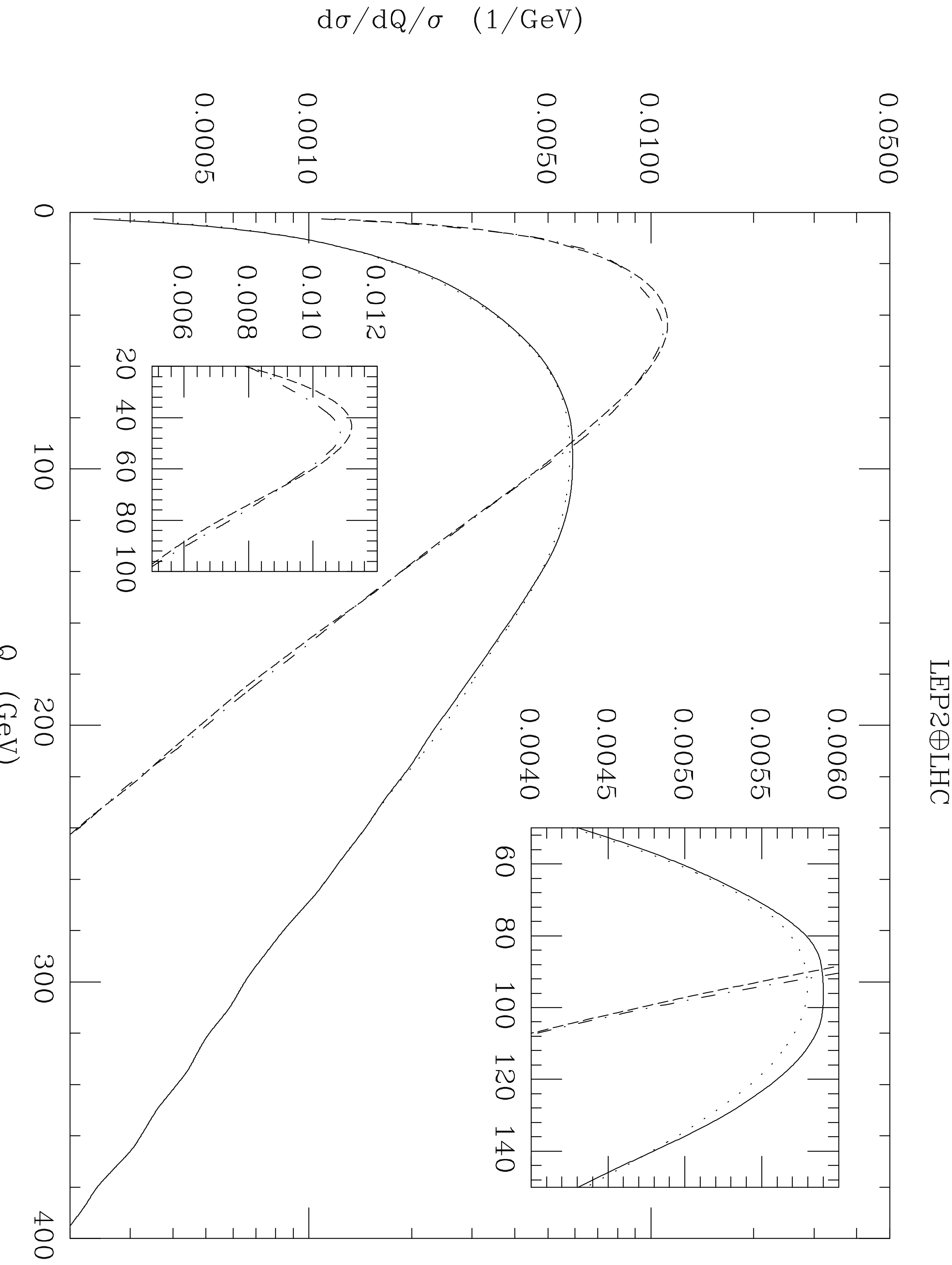

dσ/dQ/σ (1/GeV)
Q (GeV)
LEP2⊕LHC
0.0500
0.0100
0.0050
0.0010
0.0005
0
100
200
300
400
0.012
0.010
0.008
0.006
20 40 60 80 100
0.0060
0.0055
0.0050
0.0045
0.0040
60 80 100 120 140

Fig. 3b

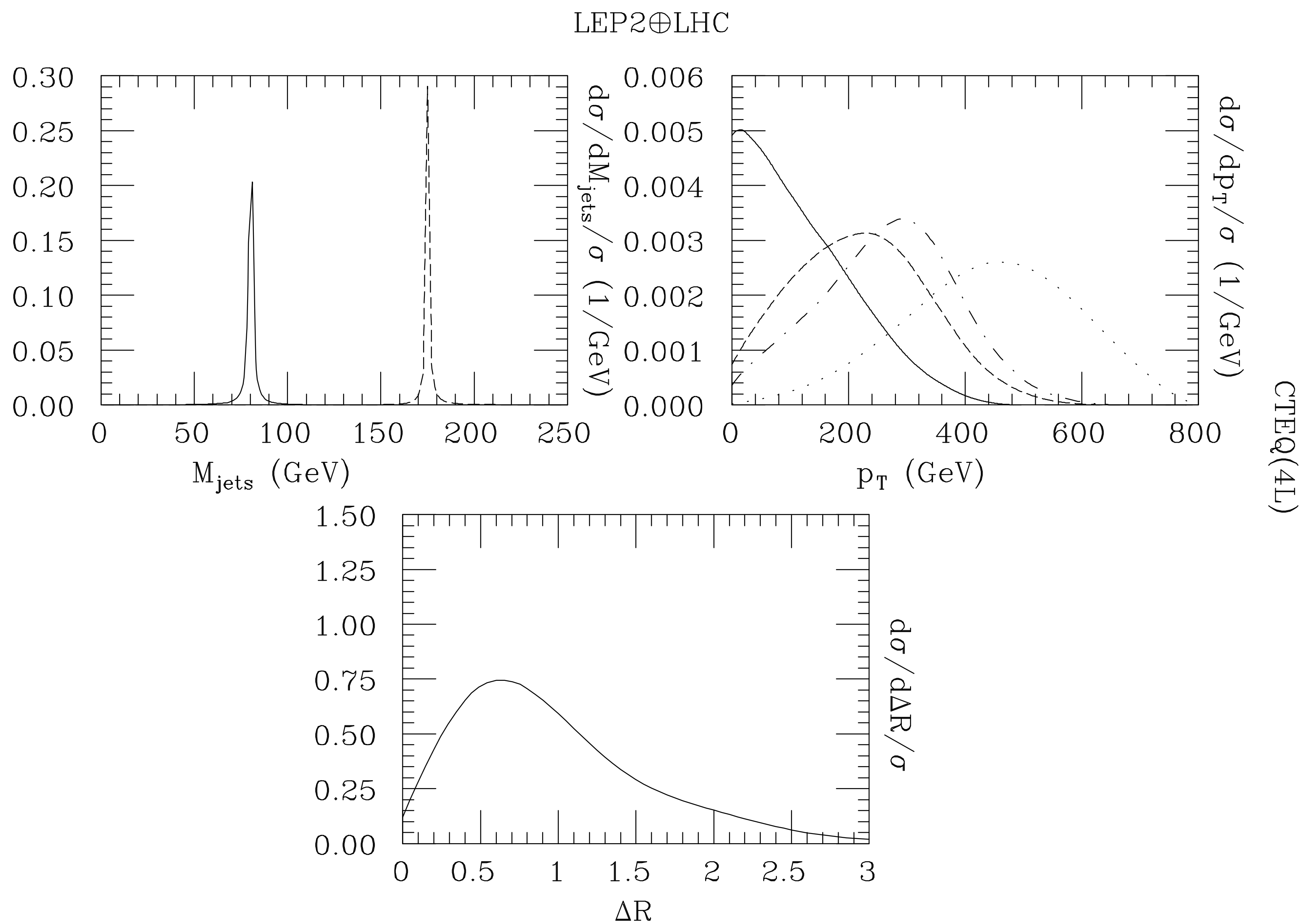

LEP2⊕LHC
CTEQ(4L)
0.00
0.05
0.10
0.15
0.20
0.25
0.30
0
50
100
150
200
250
M_jets (GeV)
dσ/dM_jets/σ (1/GeV)
0.000
0.001
0.002
0.003
0.004
0.005
0.006
0
200
400
600
800
p_T (GeV)
dσ/dp_T/σ (1/GeV)
0.00
0.25
0.50
0.75
1.00
1.25
1.50
0
0.5
1
1.5
2
2.5
3
ΔR
dσ/dΔR/σ

Fig. 4

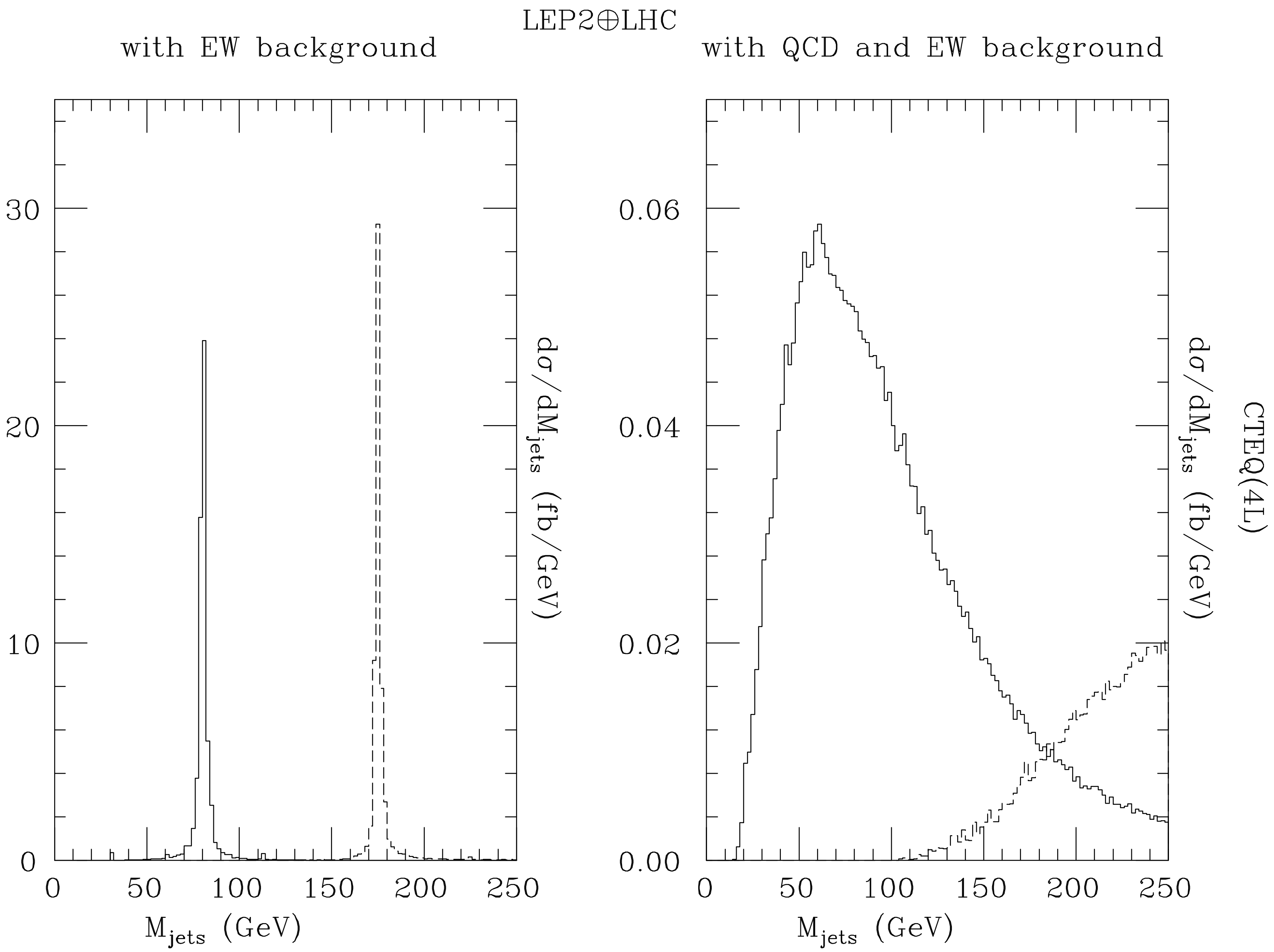
LEP2⊕LHC
with EW background
with QCD and EW background
0
10
20
30
0.00
0.02
0.04
0.06
0
50
100
150
200
250
$d\sigma/dM_{jets}$ (fb/GeV)
M_{jets} (GeV)
CTEQ(4L)

Fig. 5